NMR Investigations on Ion Dynamics and Structure in Nanocrystalline and Polycrystalline $LiNbO_3$

Detlef Bork and Paul Heitjans*

Institut für Physikalische Chemie und Elektrochemie, Universität Hannover, Callinstrasse 3-3a, 30167 Hannover, Germany

Received: June 25, 2001

Nanocrystalline (n-) $LiNbO_3$ samples with average grain sizes between 16 and 105 nm were prepared from polycrystalline (p-) material with an average grain size of the order of one micrometer by high-energy ball milling. NMR investigations of (i) the ^{7}Li spin−lattice relaxation (SLR) rate T_1^{-1} in the laboratory and T_{1e}^{-1} in the pulsed rotating reference frame and of (ii) ^{7}Li spectra, in particular line shapes and motional narrowing (MN) of the central line, were performed in the temperature range from 300 K to a maximum of 1400 K in the case of p-$LiNbO_3$ and from 140 to 460 K in the case of n-$LiNbO_3$. The following results were obtained. (1) The SLR rate measurements yield an apparent activation energy of the Li diffusion in n-$LiNbO_3$ that is about 1/3 of the value obtained for the p-material. (2) The frequency dependence of the SLR rate according to $T_{1(e)}^{-1} \propto \nu^{-\beta}$ with β in the range from 1.1 to 1.5 as well as the asymmetry of the diffusion-induced peak in the log T_{1e}^{-1} vs T^{-1} diagram of p-$LiNbO_3$ are proving non-BPP behavior for both samples. (3) In n-$LiNbO_3$ MN starts already at 250 K, i.e., about 400 K lower than in p-$LiNbO_3$, and reflects an apparent activation energy that is approximately 1/3 of the value found for the p-material. (4) In contrast to p-$LiNbO_3$, with increasing temperature the ^{7}Li NMR spectra of n-$LiNbO_3$ are revealing a characteristic structure of the central line, namely a superposition of two contributions. This is regarded as a consequence of the different dynamic properties of atoms in the interfacial regions (IR) and in the grains. From the spectrum at 450 K the fraction of atoms belonging to IR can be estimated. (5) The intensities of the quadrupole satellites showing different temperature dependencies in the p- and n-samples are indicating some exchange between the two spin reservoirs 'IR' and 'grains'. This leads to the hypothesis that n-ceramics cannot simply be regarded as heterogeneous materials where the two types of zones, i.e., IR and grains, are independent and closed.

1. Introduction

Nanocrystalline (n-) materials are (usually compacted) agglomerates of nanometer-sized crystallites with mean grain sizes ranging, approximately, from 5 to 100 nm and with random orientation of their crystallographic axes.[1,2] The small size of the crystallites implies an increased number of grain boundaries (GB) or interfacial regions (IR), in comparison with coarser grained polycrystalline (p-) systems with a typical crystallite size of some micrometers ("microcrystalline materials"). In consequence, a fraction of up to 50% of all sample atoms can be attributed to these regions. Furthermore, n-materials are mostly regarded as metastable systems with heterogeneous structural disorder consisting of two zones: randomly orientated crystallites with ideal crystal structure and disordered IR containing the system's excess energy. Reduced densities and altered coordination numbers of atoms in the IR are assumed to be responsible for the fact that n-materials are exhibiting modified or even new physical properties. In addition to the preparation of n-ceramics with varying grain sizes using high-energy ball milling, the subject of the present work is the investigation of ion dynamics, specifically diffusion, as well as the examination of structural features of n-ceramics by different nuclear magnetic resonance (NMR) techniques. We chose $LiNbO_3$ as a model system.

* To whom correspondence should be addressed. E-mail: heitjans@mbox.pci.uni-hannover.de

NMR represents a powerful tool for the characterization of dynamical[3] and structural[4] properties of solids. First we performed measurements of the temperature (T) and NMR frequency (ν) dependencies of ^{7}Li spin−lattice relaxation (SLR) rates T_1^{-1} in the laboratory and T_{1e}^{-1} in the pulsed rotating reference frame in order to study the Li diffusion in n-$LiNbO_3$ in comparison with p-$LiNbO_3$, which serves as reference material. The temperature was varied from 300 to 1400 K in the case of p-$LiNbO_3$. To prevent IR relaxation and grain growth caused by the thermal instability of n-materials at elevated temperatures, in the case of n-$LiNbO_3$ we restricted our studies to temperatures from 140 K to, at most, 460 K.

$T_{1(e)}^{-1}$ as a function of T for fixed ν generally shows a diffusion-induced peak. As is well known,[5] the position of its maximum on the temperature scale is determined by the condition $\omega\tau_c = 0.62$, where $\omega = 2\pi\nu$ is the precession frequency in the external magnetic field and τ_c is the correlation time characterizing the nuclear magnetic field fluctuations due to atomic (or ionic) diffusion at that temperature. τ_c is a measure of the mean atomic residence time between two successive jumps and is related to the diffusion coefficient D via the Einstein−Smoluchowski equation (see section 3.1). The temperature dependence of τ_c as "seen" by SLR measurements in a certain temperature range may be described by an Arrhenius relation with a pertaining activation energy E_A. In the usual log $T_{1(e)}^{-1}$ vs T^{-1} Arrhenius diagram, apparent activation energies of the Li diffusion can be determined from the slopes of the

10.1021/jp012409w CCC: $20.00
Published on Web 08/31/2001

low-temperature (E_A^{lT}) and high-temperature (E_A^{hT}) sides of the diffusion-induced peak. In contrast to the standard BPP model[6] claiming a symmetric diffusion-induced log $T_{1(e)}^{-1}$ vs T^{-1} peak, predominantly asymmetric peaks are found. In most solids the activation energy extracted from the low-temperature side turns out to be smaller than the activation energy determined from the high-temperature side. This may be ascribed to nonuniform diffusion energy barriers in a nonideal, defective solid and how they are seen by NMR relaxation with its inherent time window of the order of ω^{-1}. The activation energy E_A^{lT} from the low-T side ($\omega^{-1} \ll \tau_c$) can be attributed to the short-time limit of the diffusion process, i.e., the elementary jump, whereas E_A^{hT} should refer to long-range diffusion because at high temperatures many jumps occur before one precession of the probe spin is completed ($\omega^{-1} \gg \tau_c$).[7] Since long-range diffusion implies an increased probability to encounter and to surmount barriers of higher energy, E_A^{hT} should exceed E_A^{lT}.

Varying the NMR frequency provides information on the underlying diffusion mechanism. For example, describing the frequency dependence of the SLR rate on the low-T side by the power law $T_{1(e)}^{-1} \propto \nu^{-\beta}$, a deviation of the parameter β from the value $\beta = 2$ corresponding to standard BPP behavior reveals the influence of correlated motion and Coulomb interaction if $1 \leq \beta \leq 2$ is found.[8] We carried out SLR measurements T_1^{-1} in the laboratory reference frame at frequencies between 24 and 78 MHz. Since the above-mentioned maximum of the $T_1^{-1}(T)$ curve and the high-temperature side could not be reached below 1400 K in p-$LiNbO_3$ and 460 K in n-$LiNbO_3$, we also determined the SLR rate T_{1e}^{-1} in the pulsed rotating reference frame in the frequency range from 15 to 43 kHz.

Ion dynamics is intimately related to the structural details of the sample material. To interpret the dynamic differences expected for n- and p-$LiNbO_3$ we studied, in addition to SLR, ^{7}Li NMR spectra, in particular their temperature dependence. Previous results by our group on n-CaF_2 prepared by noble gas condensation revealed a characteristic structure of the ^{19}F NMR line: a superposition of a narrow contribution caused by mobile ions in IR and a broad contribution being ascribed to immobile ions in the grains.[9] Thus it should be possible to distinguish between the ion dynamics in the two structural zones IR and grain interior. Confirmation of these results by measurements on ball-milled samples would indicate the basic structural similarity of n-materials prepared by noble gas condensation and mechanical attrition. One aspect of the ^{7}Li NMR spectra is the temperature dependence of the line width of the central transition, i.e., the observation of motional narrowing (MN). As is well known,[5] MN of the line width starts when $\tau_c \lesssim (2\pi\delta\nu_{RL})^{-1}$, where $\delta\nu_{RL}$ is the line width of the rigid lattice, which is due to the spatial variation of the static dipolar fields. The aim is the determination of the fraction of sample atoms residing in IR from NMR spectra, which should be possible in cases where the dynamic properties of the Li probe atoms in the IR and in the grains differ significantly. This procedure might be an alternative to the well-known method based on the evaluation of XRD-line broadening (cf. section 2.2). Furthermore, as in the case of the SLR measurements, the investigation of the MN permits the calculation of an apparent activation energy for the Li diffusion. The value should correspond to E_A^{lT} rather than to E_A^{hT} because the evaluation of the line width data is normally restricted to the range $\omega^{-1} \ll \tau_c \lesssim (2\pi\ \delta\nu_{RL})^{-1}$.

A second aspect of ^{7}Li NMR spectra concerns the quadrupole satellites. While, for example, ^{19}F (cf. CaF_2 above) has a spin of 1/2 and consequently NMR spectra display a single transition, ^{7}Li NMR spectra (spin 3/2) of compounds with noncubic symmetry exhibit quadrupole satellites. It is already known from early NMR literature[10] that the degree of crystal perfection has an impact on the intensities of the quadrupole satellites in ^{7}Li NMR spectra of $LiNbO_3$. Therefore, the increasing crystal imperfection due to grain size reduction should also be detectable when comparing the intensities of the quadrupole satellites in n- and p-$LiNbO_3$ spectra. We performed corresponding investigations over a wide temperature range.

2. Experimental Section

2.1. Sample Preparation. n-$LiNbO_3$ samples were prepared by high-energy ball milling using a SPEX 8000 ball mill with an Al_2O_3 vial set. We chose Al_2O_3 because of its hardness, i.e., in order to minimize contamination of the samples caused by abrasion. The source material was p-$LiNbO_3$ with a purity of 99.99%, commercially available from Aldrich. For milling we used only one Al_2O_3 ball at a time inserted into the grinding container together with, on average, 3.8 g p-$LiNbO_3$, which corresponds to the average mass of the Al_2O_3 balls. In other words, to ensure systematic and reproducible preparation, the ratio of the mass of $LiNbO_3$ to that of the ball was kept equal to one. While loading and unloading of the vial was done in an argon atmosphere during the actual milling process, $LiNbO_3$ was in contact with air because the Al_2O_3 container delivered by SPEX is not gas tight. Although $LiNbO_3$ is not hygroscopic, the generation of IR during the milling process might cause water absorption by the n-samples to a lesser extent. By varying the milling time from 0.5 to 128 h, samples with different grain sizes were obtained. In addition, one sample was compacted at room temperature for 24 h, applying a pressure of 1.25 GPa. Furthermore, to estimate the influence of paramagnetic impurities on NMR results, two n-$LiNbO_3$ samples were prepared using a stainless steel vial set with a stainless steel ball of 8.3 g. The grinding container was filled with 8.3 g of p-$LiNbO_3$ and milling times of 8 and 16 h, respectively, were set.

2.2. Sample Characterization. According to a chemical analysis delivered by Aldrich, the p-material consists of 54.9 mol % Nb_2O_5 and 45.1 mol % Li_2O, indicating nonstoichiometry, i.e., a Li deficit, which is not unusual for lithium niobate. For example, the nonstoichiometry encountered in a congruent lithium niobate crystal grown from the melt corresponds to the composition 51.4 mol % Nb_2O_5 and 48.6 mol % Li_2O. According to the phase diagram[11] and the narrow stability range of the $LiNbO_3$ phase depicted there, the lithium niobate used in this work is made up of a predominant fraction of $LiNbO_3$ and a minor fraction of $LiNb_3O_8$, which is supported by XRD, see below. Furthermore, the material contains traces of Si (65 ppm), Na (25 ppm), W (20 ppm), Cr (6 ppm), Mg (2 ppm), and Ca (1 ppm). During n-sample preparation, weighing of the balls with an accuracy of 0.1 g serves for a crude estimation of abrasion. The latter causes the n-$LiNbO_3$ samples to contain some Al_2O_3, the content ranging between a hardly detectable amount for n-samples with small milling times and, at most, 13 wt % when milled for 128 h. Nevertheless, in routine XRD patterns, only in the case of the 128 h n-sample is there possibly a small indication for Al_2O_3 contamination (see Figure 1A). The tiny peak at $2\theta \approx 43.4°$ and the asymmetry of the peak close to $2\theta \approx 35°$ are probably caused by the most intensive lines of Al_2O_3.

XRD. The increased line width of XRD peaks caused by the reduced spatial extension of a crystal lattice to below 100 nm can be used to determine the grain size of crystalline materials.[12] Figure 1A illustrates the dependence of the XRD pattern on the milling time for $LiNbO_3$. To calculate the average grain

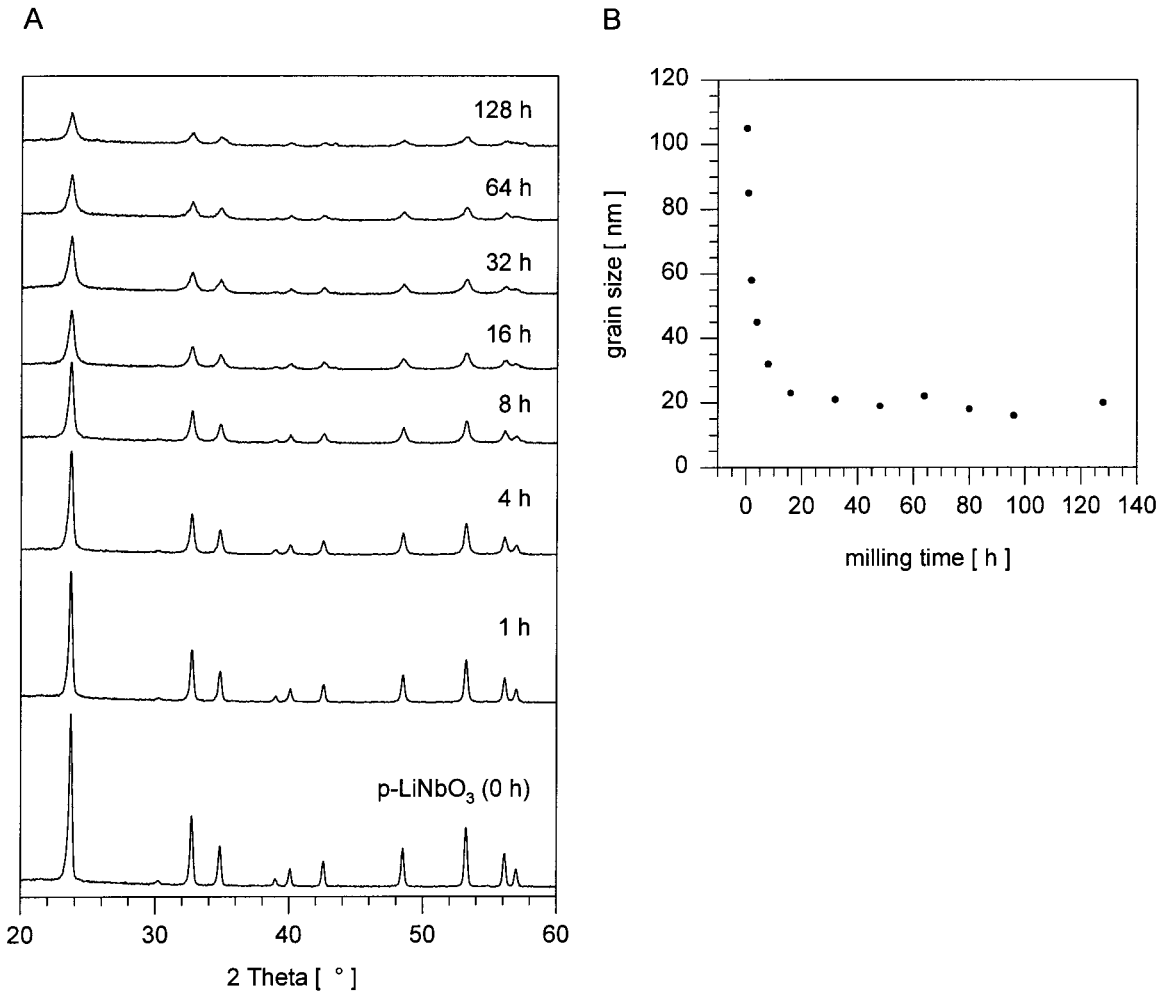

Figure 1. Milling time dependence of the $LiNbO_3$ XRD pattern (A) and the resulting average grain size determined according to Scherrer (B).

size from the XRD line width, we applied the method introduced by Scherrer, which is widely used in routine applications. The relation between the average grain size d and the width β_b of the XRD line caused by physical broadening is given by

$$d = \frac{k\lambda}{\beta_b \cos\theta} \tag{1}$$

with $\lambda = 0.154056$ nm being the wavelength of $Cu_{K\alpha 1}$-radiation, k the Scherrer constant − here assumed to be one − and θ the diffraction angle. For details of the XRD analysis, i.e., the separation of the physical and instrumental broadening of the lines, see ref 13 and references therein. As shown in Figure 1B, varying the milling time from 0.5 to 128 h yields n-$LiNbO_3$ samples with average grain sizes between 105 and 16 nm when calculated, e.g., from the diffraction peak at $2\theta = 23.7°$. With the assumption that the average IR thickness ranges from 0.5 to 1 nm it is possible to calculate the fraction of the sample atoms residing in IR^2. In the case of the n-$LiNbO_3$ sample ball-milled for 16 h with a resulting grain size of 23 nm, one obtains fractions ranging from 5% to 8%. The small peak at $2\theta \approx 30°$ in the XRD pattern of p-$LiNbO_3$ (Figure 1A) is caused by a small fraction of $LiNb_3O_8$.[14] This reflects the above-mentioned nonstoichiometry of the source material.

TEM. In addition to XRD which, strictly spoken, only gives information about the size of coherent scattering areas, TEM is able to resolve structural details such as single nanocrystals. Whereas the broadening of XRD lines is usually caused by lattice distortions and/or stacking faults etc., grain size reduction becomes the dominating factor in samples with average grain diameters below 100 nm. In this case other influences can be neglected.[12] To ensure that the grain sizes determined from XRD were due to grain size reduction, TEM images were taken. In contrast to the p-$LiNbO_3$ sample consisting of irregular shaped crystallites of grain sizes between 0.6 and 6 μm, the n-$LiNbO_3$ sample ball-milled, e.g., for 16 h, is made up of agglomerates of more regularly shaped grains with an average diameter of approximately 27 nm, which agrees with the value of 23 nm obtained from XRD. Therefore, the TEM results justify the underlying assumptions concerning the XRD analysis. A characteristic structural element of n-$LiNbO_3$ samples prepared by ball-milling seems to be large-angle GB separating nanometer-sized grains. As a consequence, there is no correlation between the crystallographic orientation of neighboring crystals. This is a first hint that preparing nanocrystalline ceramics via ball-milling is able to produce materials structurally similar to those obtained through noble gas condensation.

DTA. Thermal properties of the n-sample, ball-milled for 16 h yielding a grain size of 23 nm, were examined by DTA in the temperature range from 300 to 960 K at a heating rate of 20 K/min, in comparison with p-$LiNbO_3$. Whereas p-$LiNbO_3$ showed no significant thermal effect, the n-sample exhibits the onset of an exothermic signal at about 510 K revealing GB relaxation and grain growth, which are almost completed at 960 K. Because these processes have no specific transition temperatures and DTA is a dynamical method, the temperature range

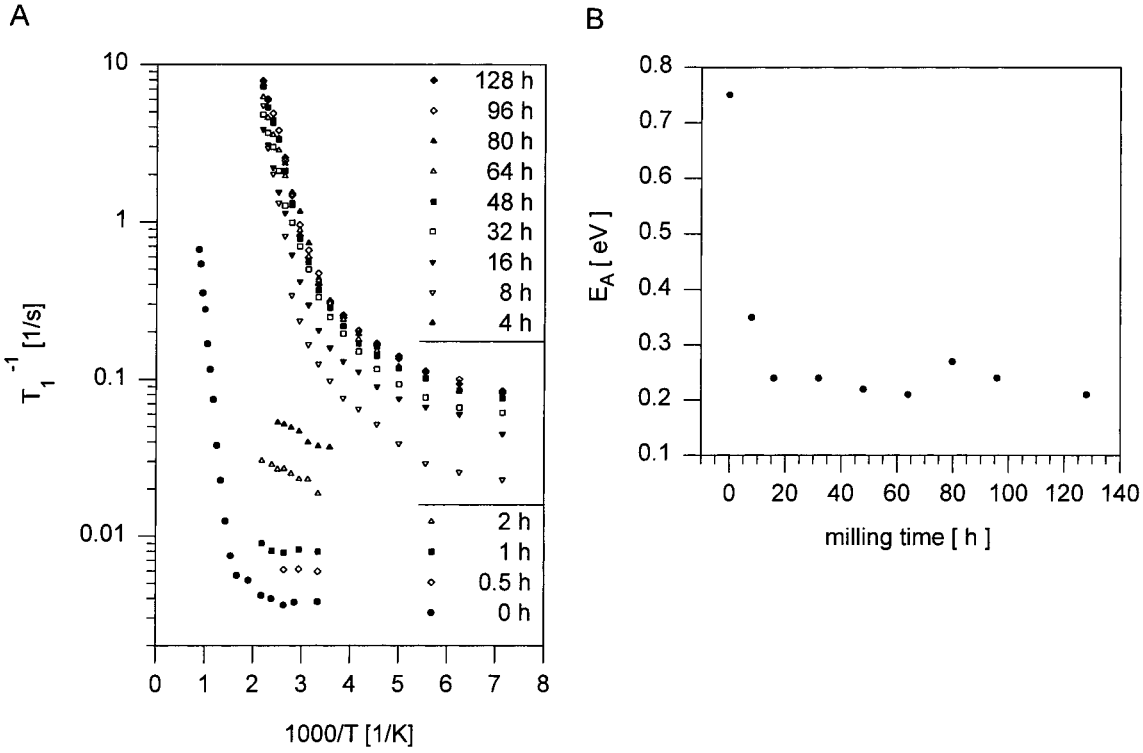

Figure 2. Arrhenius diagram displaying the temperature dependence of the ^{7}Li SLR rate T_1^{-1} in n-$LiNbO_3$ at 39 MHz for various milling times (A) and the resulting diffusion activation energies (B).

below 510 K cannot be identified with an actual thermal stability range of the n-sample. In fact, we found that NMR experiments had to be restricted to temperatures below 460 K. At higher temperatures the time intervals required for NMR-data acquisition already enable irreversible relaxation and grain growth.

2.3. NMR Measurement Conditions. The measurements of the SLR time T_1 of ^{7}Li in the laboratory reference frame at 24 and 39 MHz were performed using a Bruker MSL 100 console with an internal 200 W power amplifier and a tunable Oxford 7 T cryomagnet with an 89 mm bore. For T_1 experiments at 78 MHz, the determination of the SLR time T_{1e} in the pulsed rotating reference frame, the acquisition of the ^{7}Li NMR spectra, and investigation of the MN, we used a Bruker MSL 200 spectrometer with an internal 200 W amplifier and an Oxford cryomagnet at fixed field. Measurements in the temperature range from 140 to 460 K were carried out using commercial Bruker probe heads while temperatures up to 1400 K were attained through home-built probe heads. In the investigated frequency range, p-$LiNbO_3$ shows SLR times T_1 up to a few hundred seconds. From a practical point of view, one has to apply time saving pulse sequences such as the saturation recovery pulse sequence ($n\cdot\pi/2 - \tau - \pi/2$) for measurements in the laboratory reference frame.[15] Measurements in the kHz regime were performed using the T_{1e} pulse sequence, which implies a pulsed rotating reference frame. According to ref 16, this pulse sequence is a time saving alternative to conventional $T_{1\rho}$ experiments being performed in a continuously rotating reference frame. In the T_1 measurements on both the p- and n-samples, as well as in the case of the T_{1e} experiments on p-$LiNbO_3$, no significant deviation of the time evolution of the magnetization from single-exponential behavior could be detected. In contrast, the transients in the T_{1e} experiments on n-$LiNbO_3$ rather followed a stretched exponential[17] which meets the expectation that a system consisting of two different structural zones should not show single-exponential relaxation. The reason that in the case of the T_1 measurements on n-$LiNbO_3$ stretched or, ideally, double-exponential SLR, could not be detected (whereas the NMR line shapes did reflect the heterogeneous structure and dynamics, see section 3.3) can be ascribed to the fact that under the present conditions the two relaxation-time values were too far apart.

3. Results

3.1. Spin-Lattice Relaxation. *n-$LiNbO_3$.* Figure 2A displays the temperature dependence of the ^{7}Li SLR rate T_1^{-1}, measured at 39 MHz, for 12 n-$LiNbO_3$ samples with different milling times in comparison with the polycrystalline source material (0 h). In each case, T_1^{-1} consists of a diffusion-induced SLR rate that sharply rises with increasing temperature to the expected maximum and of a nondiffusive "background" SLR rate, which shows up at low temperatures and has no or only a weak T dependence. The SLR rate background has negligible influence on the data at the highest temperatures, whose slope yields the "low-T side" activation energy E_A^{IT} (cf. section 1), and will not further be analyzed here. With increasing milling time, the $T_1^{-1}(T)$ curves shift to lower temperatures and the SLR rate background rises. The shift indicates that with decreasing grain size Li diffusion is starting at lower temperatures. For milling times longer than 48 h, the curves almost coincide. The enhanced diffusivity is reflected by a reduction of the activation energy E_A^{IT} from 0.75 eV in p-$LiNbO_3$ to approximately 0.23 eV in n-$LiNbO_3$, which can be regarded as a "saturation limit" as seen from Figure 2B. The necessity to restrict NMR experiments to temperatures below 460 K, as stated above, prevents the detection of the sharp rise of T_1^{-1} with increasing T in n-samples ball-milled for less than 8 h. Considering that especially the samples milled for 96 and 128 h are contaminated with up to 13 wt % Al_2O_3 the saturation concerning the growing ^{7}Li SLR rates and the decreasing activation energies with increasing milling times proves that the influence of impurities

contained in ball-milled n-samples on NMR results is limited. Similar results, not displayed here, were obtained from corresponding ^{7}Li SLR rate measurements on n-$LiNbO_3$ samples prepared with a stainless steel vial set. Milling times of 8 and 16 h yielded grain sizes of 28 and 26 nm, respectively; the resulting activation energies are 0.25 and 0.22 eV. As far as the diffusion-induced low-temperature side is concerned, there are no significant deviations of the $T_1^{-1}(T)$ curves belonging to the samples prepared in the Al_2O_3 from those in the steel vial set. Only the background SLR rate is slightly increased in the "steel samples", probably caused by paramagnetic impurities. Furthermore, the compaction (pressure: 1.25 GPa) of the above-mentioned n-sample ball-milled for 16 h in the Al_2O_3 vial set revealed no effect on the ^{7}Li SLR rate when compared with the as-prepared, i.e., not compacted sample. The latter sample was used to perform measurements at various frequencies as shown in Figure 3A. The frequency dependence of the ^{7}Li SLR rate T_1^{-1} in the laboratory reference frame can be described by the power law $T_1^{-1} \propto \nu^{-\beta}$. The value of $\beta = 1.1$, determined on the low-temperature side, indicates the influence of structural disorder and coulomb interaction between the diffusing Li ions as stated, e.g., by the jump-relaxation model.[8] The value 0.27 eV for the activation energy, being obtained from the data points at the highest temperatures that show Arrhenius behavior, is independent of frequency but has to be regarded as a lower limit because it is not evident that the steepest part of the low-temperature side is already reached at 460 K (see also the result from MN below). Measurements of the SLR rate T_{1e}^{-1} in the pulsed rotating reference frame between 15 and 24 kHz can only detect the very beginning of the Li diffusion (see ref 17, Figure 4) and therefore yield no additional information.

p-$LiNbO_3$. Because no suitable SLR data are reported in the literature, extensive measurements on p-$LiNbO_3$ had to be performed in order to define an "internal reference", i.e., a relative standard, for the interpretation (cf. section 1). The results of the ^{7}Li SLR rate experiments $T_1^{-1}(T)$ obtained in the laboratory reference frame are shown in Figure 3B, whereas Figure 3C displays a selection of data resulting from T_{1e}^{-1} measurements in the pulsed rotating reference frame. In both reference frames, an activation energy of 0.75 eV, which is independent of the frequency, can be determined from the steepest part of the respective low-temperature side, whereas an activation energy of 0.88 eV can be extracted from the slope of the high-temperature side visible in the $T_{1e}^{-1}(T)$ plot. Following the arguments on the different aspects of dynamical processes probed by SLR in the limiting cases $\omega^{-1} \ll \tau_c$ and $\omega^{-1} \gg \tau_c$ given in the Introduction, the two values for the activation energy can be attributed to the short-range and long-range motion, respectively, of the Li ions. Furthermore, from the condition $\omega\tau_c = 0.62$ for the maximum of the log T_{1e}^{-1} vs T^{-1} peak and the Einstein−Smoluchowski equation for three-dimensional diffusion the self-diffusion coefficient D can be calculated:

$$D = \frac{\langle r^2 \rangle}{6\tau_c} \qquad (2)$$

Here $\langle r^2 \rangle$ is the mean-square displacement of the elementary jump. If for r the Li−Li distance in the crystal structure of $LiNbO_3$ of about 0.38 nm[18] is adopted, one finds for $T = 890$ K with $\omega = 1.9 \times 10^5$ s^{-1}, i.e., $\tau_c = 3.3 \cdot 10^{-6}$ s, $D(890\ \mathrm{K}) = 7.3 \times 10^{-15}$ m^2/s

The frequency dependences of the SLR rate of $\beta = 1.2$ found in the MHz range and $\beta = 1.5$ in the kHz regime can, in analogy

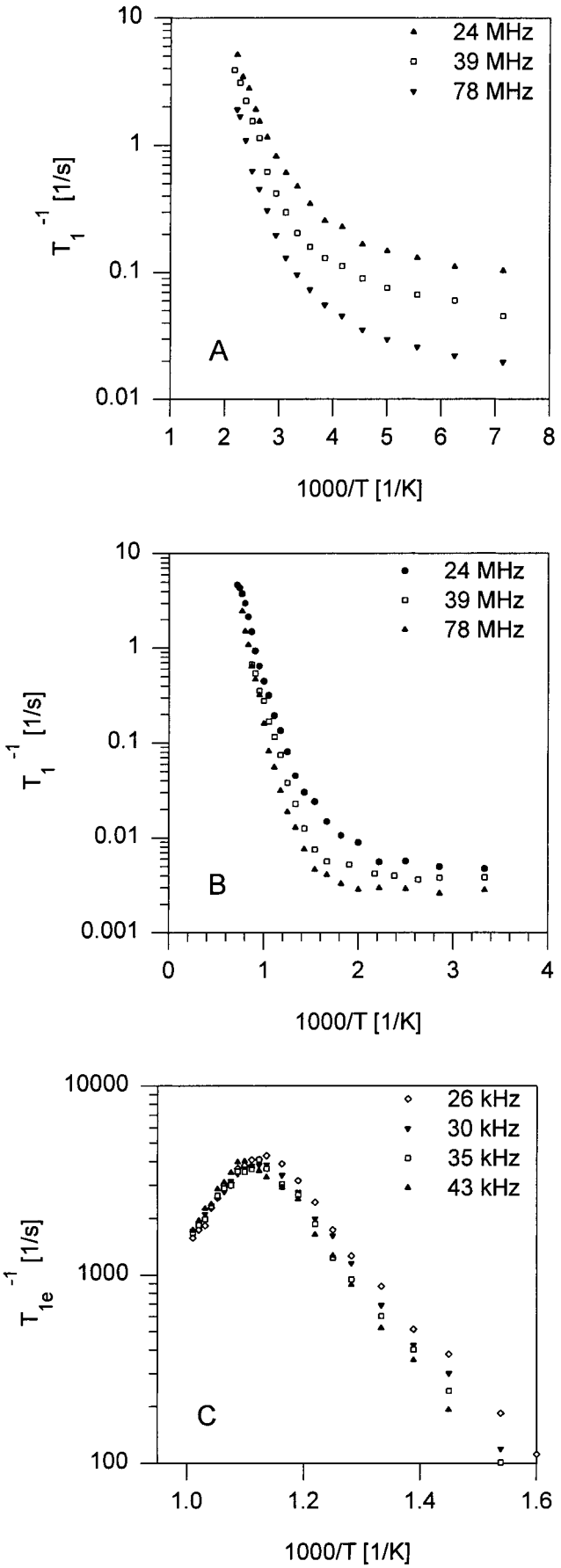

Figure 3. Temperature dependence at various frequencies of the ^{7}Li SLR rate T_1^{-1} in n-$LiNbO_3$ milled for 16 h with a resulting average grain size of 23 nm (A), in p-$LiNbO_3$ (B), and of the ^{7}Li SLR rate T_{1e}^{-1} in p-$LiNbO_3$ (C).

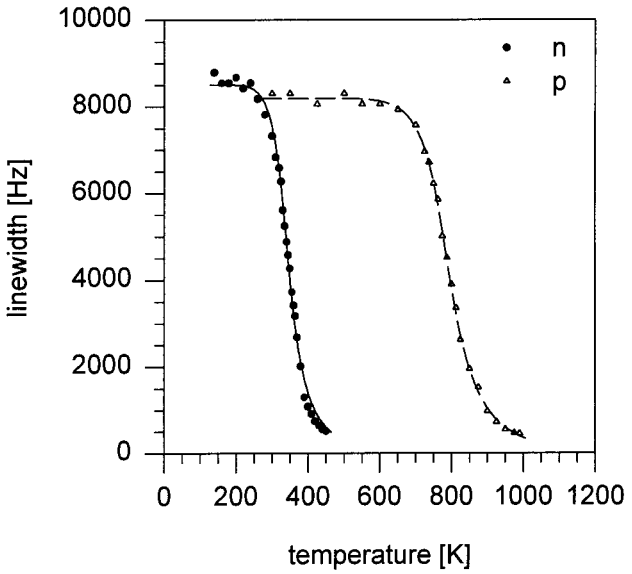

Figure 4. Temperature dependence of the line width of the central transition (MN) in the ^{7}Li NMR spectra of n- and p-$LiNbO_3$ obtained at 78 MHz. The lines through the data points represent fits according to eq 4.

to n-$LiNbO_3$, be interpreted, e.g., in terms of the jump-relaxation model.[8] This is also true for the asymmetric peaks observed in the $T_{1e}^{-1}(T)$ curves in Figure 3C. On the other hand, the jump-relaxation model, among others, claims a relation between the activation energies E_A^{lT} and E_A^{hT} obtained from the low- and high-temperature side, respectively, and the parameter β characterizing the frequency dependence of the SLR rate (cf., e.g., ref 3, p 120):

$$\frac{E_A^{lT}}{E_A^{hT}} = \beta - 1 \qquad (3)$$

Insertion of the experimental values clearly shows that eq 3 does not hold for p-$LiNbO_3$. Thus, while our SLR results qualitatively agree with, e.g., the jump-relaxation model, a more detailed analysis reveals deviations between theory and experiment.

The absence of a frequency dependence of the SLR rate T_{1e}^{-1} on the high-temperature side proves that diffusion is isotropic, i.e., three-dimensional, as assumed in eq 2.[7] This contrasts with, e.g., polycrystalline hexagonal Li_xTiS_2 where SLR studies showed that Li diffusion is two-dimensional.[19] Unlike $LiNbO_3$, E_A^{lT} in nanocrystalline Li_xTiS_2 is not significantly smaller than in the polycrystalline form.[20]

3.2. Spectra: Motional Narrowing. Further insight concerning the differences in the dynamic behavior of n- and p-$LiNbO_3$ is gained by the investigation of the temperature dependence of the central transition line width (fwhm) in ^{7}Li NMR spectra. Our results obtained at 78 MHz from measurements on the n-sample ball-milled for 16 h and on the p-sample are compared in Figure 4. The onset of MN is shifted by more than 400 K from 650 K in p-$LiNbO_3$ to below 250 K in the n-sample. Moreover, in the n-material MN is nearly completed at 450 K. Thus, the examination of MN represents an alternative method to determine apparent activation energies for the Li diffusion. The lines through the data points in Figure 4 represent fits according to the ad hoc formula given in ref 21

$$\delta\nu(T) = \sqrt{\delta\nu_{RL}^2 \frac{2}{\pi} \arctan\left[\alpha\delta\nu(T)\tau_\infty \exp\left(\frac{E_A}{kT}\right)\right] + \delta\nu_\infty^2} \qquad (4)$$

from which the activation energies E_A were calculated. $\delta\nu$ is the width of the central line at the temperature T, $\delta\nu_{RL}$ its respective width in the rigid lattice, and $\delta\nu_\infty$ the residual line width caused by nondipolar interactions when the MN is completed. α represents a fit parameter here chosen to be one. τ_∞ is the preexponential factor in the Arrhenius relation assumed for the temperature dependence of the correlation time τ_c. For further aspects see ref 21. In agreement with the SLR results obtained from the slope of the low-temperature T_1^{-1} flanks for 78 MHz, the activation energy derived from MN in p-$LiNbO_3$ is reduced to approximately 1/3 in n-$LiNbO_3$, viz. from 0.83 to 0.26 eV.

3.3. Spectra: Line Shapes. Supported by the ^{7}Li NMR spectra, it is possible to relate the observed dynamical features to the structural properties of the sample. In Figure 5, spectra of p-$LiNbO_3$ (left-hand side) are displayed facing spectra of n-$LiNbO_3$ (right-hand side) in "equivalent dynamical states", which are characterized by comparable line widths of the central transitions. The distinct dynamical properties of the p- and n-$LiNbO_3$ samples are responsible for the different temperatures at which the respective spectra facing each other were obtained. Figure 5A displays the spectrum of the rigid lattice in p-$LiNbO_3$ measured at 550 K, which is compared with the spectrum of n-$LiNbO_3$ at 160 K shown in Figure 5B. Whereas in p-$LiNbO_3$ the two quadrupole satellites are resolved as individual lines, in n-$LiNbO_3$ they show up as pronounced shoulders close to the central line. The reason is the temperature dependence of the quadrupole splitting in $LiNbO_3$, i.e., the difference $\Delta\nu$ between the frequencies belonging to the respective peak of the satellites, which grows with increasing temperature. According to Halstead,[22] this temperature dependence can be explained by an anisotropic vibration of light atoms.

Figures 5C and 5D show the spectra after MN is completed in both samples, i.e., at 975 K in p-$LiNbO_3$ and at 450 K in n-$LiNbO_3$. The satellites have vanished in n-$LiNbO_3$ at 450 K, while in p-$LiNbO_3$ at 975 K they are still visible. Corresponding to the progressive MN and the growing quadrupole splitting with increasing temperature, the quadrupole satellites become more and more separated from the central line, allowing the quantification of the splitting in the powder sample with only minor errors. In p-$LiNbO_3$ we find $\Delta\nu = (36 \pm 0.5)$ kHz at 975 K. Thus, for the quadrupole coupling constant $e^2qQ/h = 2\Delta\nu$[23,24] the value (72 ± 1) kHz at 975 K is obtained. This is in agreement with results from refs 22 and 25, respectively, when the inherent limitations of a precise determination of the stoichiometry of $LiNbO_3$ samples (cf. section 4) are taken into account.

In Figures 5E and 5F, the central lines being determined by dipole−dipole interaction are plotted on an enlarged scale in order to reveal the characteristic structure of the central line in the n-$LiNbO_3$ spectrum. In contrast to the "single-line structure" obtained for p-$LiNbO_3$, the central line of the n-material is composed of two distinct contributions, namely, a narrow line superimposed on a broad line at the same central frequency.

4. Discussion

For the discussion of the NMR results some additional remarks concerning the properties of $LiNbO_3$ will be useful. The chemical formula $LiNbO_3$ describes an idealized stoichiometric system. In fact, lithium niobate is nonstoichiometric[26] (cf. section 2.2). The nonstoichiometry involves a defect structure that is still under investigation, see, e.g, refs 27 and 28. Among other physical properties, the ^{93}Nb NMR resonance (ref 26 and references therein) and the quadrupole splitting of

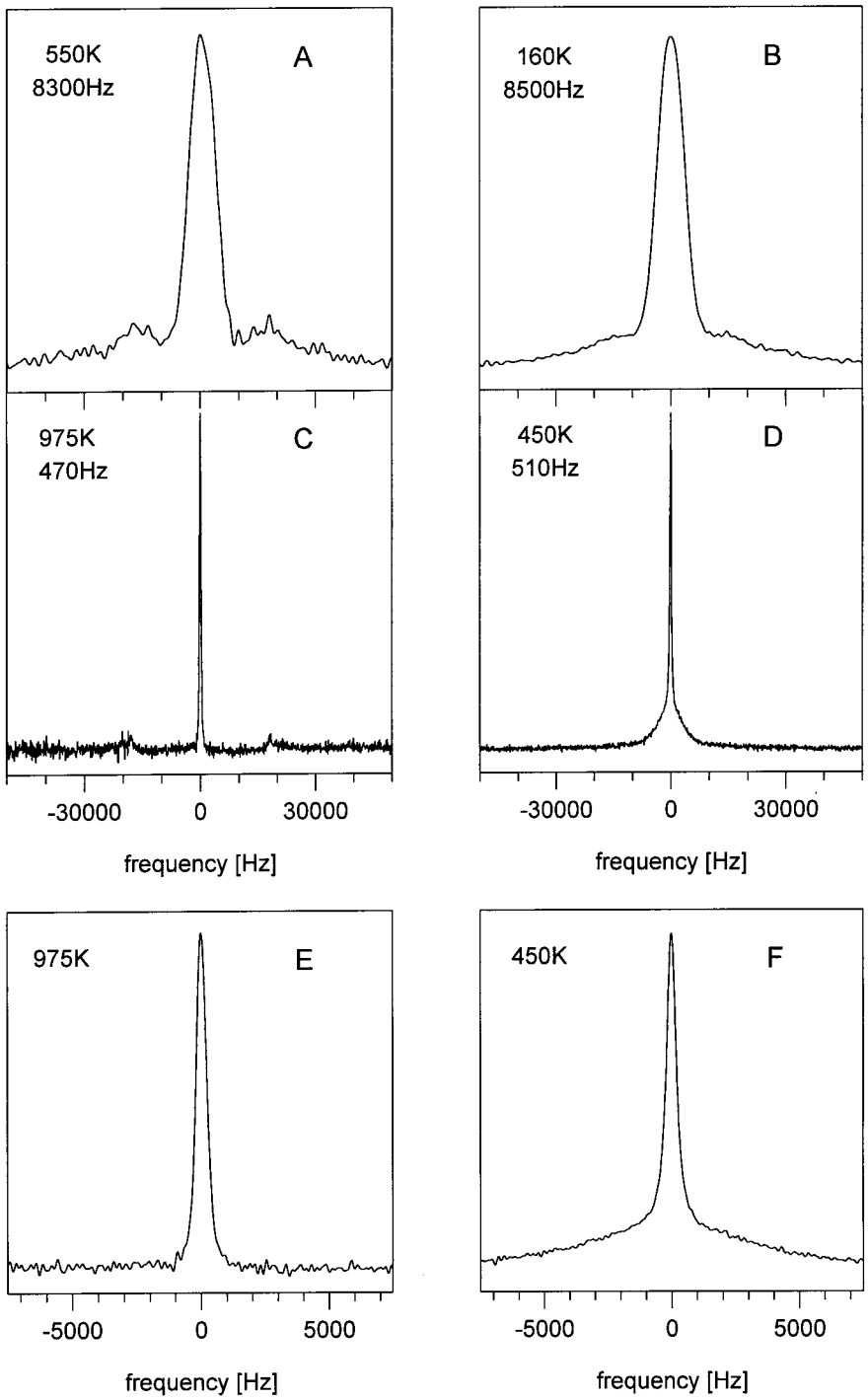

Figure 5. Comparison of the ^{7}Li NMR spectra of p-$LiNbO_3$ (left) and n-$LiNbO_3$ (right) in different dynamical regimes, i.e., in the rigid lattice (A, B) and after the MN is completed (C, D). Characteristic structural features of the samples are revealed by the shapes of the central lines (E, F).

the ^{7}Li NMR spectrum[25] are sensitive to stoichiometry. In principle these properties could be used for a precise determination of the stoichiometry of $LiNbO_3$ samples. A prerequisite is the availability of at least one calibrated standard. On the other hand, it is known from the literature that a quantitative chemical analysis with the required degree of precision is hardly obtainable.[26] Therefore, no reliable standard for, e.g., the use of the ^{7}Li quadrupole splitting can be found in the literature yet. Furthermore, regarding the phase diagram,[11] $LiNbO_3$ grown from a nonstoichiometric congruent melt is inherently metastable at lower temperatures. These characteristics imply limits concerning the interpretation of the data and restrictions when comparing them with other results from the literature. This is another reason the p-material is used as an "internal reference", i.e., serves as a relative standard for the interpretation of the results obtained from measurements on the n-samples.

First Halstead[22] investigated the Li diffusion in a $LiNbO_3$ single crystal by recording the MN. He reported an activation energy of 1.62 eV for the Li diffusion occurring above 820 K. According to our results, the activation energy is between 0.75 and 0.88 eV, as determined from the SLR and MN experiments on p-$LiNbO_3$. Furthermore, our results cannot support the interpretation[22] suggesting a second mechanism, e.g., a to-and-fro motion with a reduced activation energy, prevailing at temperatures below 820 K; we found experimental evidence only for one diffusion process in p-$LiNbO_3$.

The enhanced Li diffusivity in n-$LiNbO_3$ as compared to the p-system, which is also reflected by the reduced activation energies determined from the SLR and MN data, can be ascribed to the atoms residing in the IR. The degree to which the dynamic behavior of Li ions in the IR differs from that of the ions in the interior of the grains can be seen from the pronounced shift of the MN by more than 400 K to lower temperatures in n-$LiNbO_3$. Furthermore, MN is completed 200 K below the temperature where it starts in the p-material. The interpretation that only atoms in the IR are mobile at, e.g., 450 K whereas the ions in the grains are still immobile is suggested by the corresponding ^{7}Li NMR spectrum of n-$LiNbO_3$. As can be seen in Figure 5F, the central line at 450 K shows the superposition of two contributions mentioned before: (i) a narrow line caused by the atoms in the IR and (ii) a broad part caused by the immobile ions in the grains. Of course, at still higher temperatures, the ions in the grains become mobile and the broad part of the line should show MN. Observation of MN, however, was prevented by the restricted thermal stability of the n-samples.

The distinct structure of the central line in the 450 K spectrum of n-$LiNbO_3$ offers a possibility to determine the fraction of Li ions that can be ascribed to IR. Assuming that the ratio of the area of the narrow NMR line to that of the total line is equal to the fraction of atoms risiding in IR, about 23% of the atoms of the n-sample ball-milled for 16 h (average grain size 23 nm) are found to belong to IR. This is in contrast to the values 5−8% calculated from XRD data according to ref 2, see below.

The investigation of the influence of the *heterogeneous* structural disorder on the diffusive motion in n-$LiNbO_3$ by exploring the frequency dependence of the SLR rate fails because of the *homogeneous* disorder being additionally present. The latter is caused by the above-mentioned defect structure resulting from the inherent nonstoichiometry and is already present in p-$LiNbO_3$, i.e., in the source material for the preparation of the n-samples. Thus, in the case of n-$LiNbO_3$, both the grains and the IR have highly defective or disordered structures and their influence on the frequency dependence of the diffusion induced SLR rate will be similar.

The symmetric shape of the central line in p-$LiNbO_3$, in the case of completed MN involving a residual line width of about 450 Hz (Figure 5C,E) is in agreement with a magic-angle spinning (MAS) NMR investigation by Blümel et al.[27] Their aim was to distinguish between different models for the defect structure of $LiNbO_3$, predicting two distinct Li sites occupied by different fractions of Li ions, i.e., two neighboring ^{7}Li NMR lines with varying relative intensities. Although they reduced the line width to 600 Hz, a second ^{7}Li line could not be detected.

As stated in the Introduction the impact of crystal imperfection on the intensities of quadrupole satellites in $LiNbO_3$ has already been discussed in the literature.[10] It is reported that the intensities of the satellites are diminished with reduced crystal perfection, independent of whether it is caused by chemical or physical defects, e.g., by impurities, vacancies, and/or dislocations. Nevertheless, assuming the spin reservoirs IR and grains are independent of each other, at 450 K quadrupole satellites should still be detectable in n-$LiNbO_3$ because of the following arguments. First, they can be identified in the 160 K spectrum of n-$LiNbO_3$ (Figure 5B), proving that pure grain size reduction, i.e., when ^{7}Li diffusion is absent, does not lead to vanishing quadrupole satellites. Second, about 77% of the atoms of the n-sample can be attributed to the grain interior, which, according to the underlying assumption, is supposed to behave like the p-material. Therefore, third, this contribution to the overall signal should not vanish below 975 K, as seen from the corresponding p-$LiNbO_3$ spectrum. This is why our results seem to indicate some exchange between the spin reservoirs and that n-materials cannot strictly be regarded as heterogeneous systems built up by two types of independent zones.

Furthermore, an interaction of both zones influencing the dynamic properties might also be responsible for the above-mentioned disagreement when calculating the fraction of atoms residing in IR from NMR spectra and XRD data, respectively. On the other hand, one could imagine that, in addition to the IR, the grain interior of the n-material has a high defect concentration which exceeds that of the grains in the p-material. As a consequence, at elevated temperatures NMR would possibly detect a larger fraction of ions being mobile than one would expect when just calculating the fraction of atoms that belong to IR from XRD data obtained at room temperature.

5. Conclusions

Ball-milling serves as a useful method for the systematic and reproducible preparation of ceramic samples with variable grain sizes in the nanometer region. The enhanced Li diffusivity in n-$LiNbO_3$ involving a reduced activation energy as determined from SLR and MN experiments can be ascribed to the Li ions residing in the interfacial regions. The different dynamic behavior of Li ions in the interfacial regions and in the crystallites is verified by the complementary information extracted from temperature-dependent NMR spectra, i.e., ^{7}Li NMR line shape studies and the observation of the MN of the central lines. Nevertheless, we found experimental indications that the spin reservoir "grains" and "interfacial regions" are not independent of each other but exhibit some exchange not yet specified in detail. Further research work concerning this aspect is required.

Acknowledgment. We thank Dr. G. Balzer for useful discussions concerning NMR aspects. The XRD and DTA measurements were performed by Dr. J. Beyer, the TEM images were delivered by Prof. S. Rahman. This work was supported by the Deutsche Forschungsgemeinschaft (DFG) and the Fonds der Chemischen Industrie.

References and Notes

(1) Gleiter, H. *Prog. Mater. Sci.* **1989**, *33*, 223.
(2) Siegel, R. W. In *Encyclopedia of Applied Physics*; Trigg, G. L., Immergut, E. H., Vera, E. S., Greulich, W., Eds.; VCH: New York, 1994; Vol. 11, p 173.
(3) *Diffusion in Condensed Matter*; Kärger, J., Heitjans, P., Haberlandt, R., Eds.; Vieweg: Braunschweig, Springer: Berlin, 1998.
(4) *Solid State NMR I, III, IV*; Blümich, B., Ed. (*NMR Basic Principles and Progress* Vols. 30, 32, 33; Diehl, P.; Fluck, E.; Günther, H.; Kosfeld, R.; Seelig, J., Eds.); Springer: Berlin, 1994.
(5) Slichter, C. P. *Principles of Magnetic Resonance*; Springer: Berlin, 1990.
(6) Bloembergen, N.; Purcell, E. M.; Pound, R. V. *Phys. Rev.* **1948**, *73*, 679.
(7) Heitjans, P.; Schirmer, A. In *Diffusion in Condensed Matter*; Kärger, J., Heitjans, P., Haberlandt, R., Eds.; Vieweg: Braunschweig, Springer: Berlin, 1998; p 116.
(8) Funke, K. *Prog. Solid State Chem.* **1993**, *22*, 111.
(9) Puin, W.; Heitjans, P.; Dickenscheid, W.; Gleiter, H. In *Defects in Insulating Materials*; Kanert, O., Spaeth, J., Eds.; World Scientific: Singapore, 1993; p 137.
(10) Bogdanov, V. L.; Lemanov, V. V.; Klyuev, V. P.; Fedulov, S. A. *Sov. Phys. Solid State* **1968**, *10*, 886.
(11) Svaasand, L. O.; Eriksrud, M.; Grande, A. P.; Mo, F. *J. Cryst. Growth* **1973**, *18*, 179.
(12) Klug, H. P.; Alexander, L. F. *X-ray Diffraction Procedures*; John Wiley and Sons: New York, 1974.
(13) Bork, D. Dissertation, Universität Hannover, 1997.
(14) Leroux, C.; Nihoul, G.; Malovichko, G.; Grachev, V.; Boulesteix, C. *J. Phys. Chem. Solids* **1998**, *59*, 311.

(15) Fukushima, E.; Roeder, S. B. W. *Experimental Pulse NMR*; Addison-Wesley: London, 1981.
(16) Rhim, W.-K.; Burum, D. P.; Ellemann, D. D. *J. Chem. Phys.* **1978**, *68*, 692.
(17) Bork, D.; Heitjans, P. *J. Phys. Chem. B* **1998**, *102*, 7303.
(18) *Gmelins Handbuch der Anorganischen Chemie*, Niob, Teil B 4 (Verlag Chemie Weinheim/Bergstr. 1973).
(19) Küchler, W.; Heitjans, P.; Payer, A.; Schöllhorn, R. *Solid State Ionics* **1994**, *70/71*, 434.
(20) Winter, R.; Heitjans, P. *J. Phys. Chem. B* **2001**, *105*, 6108.
(21) Abragam, A. *The Principles of Nuclear Magnetism*; Clarendon: Oxford, 1961.
(22) Halstead, T. K. *J. Chem. Phys.* **1970**, *53*, 3427.
(23) Cohen, M. H.; Reif, F. In *Solid State Physics*; Seitz, F., Turnbull, D., Eds.; Academic Press: New York, 1957; Vol. 5, p 321.
(24) Peterson, G. E.; Bridenbaugh, P. M.; Green, P. *J. Chem. Phys.* **1967**, *46*, 4009.
(25) Charnaya, E. V.; Gabrielyan, V. T.; Kasperovich, V. S.; Klimko, S. *Phys. Solid State* **1996**, *38*, 1041.
(26) Räuber, A. Chemistry and Physics of Lithium Niobate in *Current Topics in Materials Science*; Kaldis, E., Ed.; North-Holland: Amsterdam, 1978; Vol. 1.
(27) Blümel, J.; Born, E.; Metzger, T. *J. Phys. Chem. Solids* **1994**, *55*, 589.
(28) Kong, Y.; Xu, J.; Chen, X.; Zhang C.; Zhang, W.; Zhang, G. *J. Appl. Phys.* **2000**, *87*, 4410.